Title: Cortico-cortical and hippocampo-cortical co-rippling are facilitated by thalamo-cortical spindles and upstates, but not by thalamic ripples

Abbreviated title: Thalamic ripples in humans

Authors: Charles W. Dickey[1,2,*], Ilya A. Verzhbinsky[1,2], Sophie Kajfez[3], Burke Q. Rosen[1], Sandipan Pati[4,†], Eric Halgren[3,5,*,†]

[1]Neurosciences Graduate Program, University of California San Diego, La Jolla, CA 92093
[2]Medical Scientist Training Program, University of California San Diego, La Jolla, CA 92093
[3]Department of Radiology, University of California San Diego, La Jolla, CA 92093
[4]Department of Neurology, University of Texas Health Science Center, Houston, TX 77030
[5]Department of Neurosciences, University of California San Diego, La Jolla, CA 92093

*Corresponding authors: Charles W. Dickey (cdickey@health.ucsd.edu) and Eric Halgren (ehalgren@health.ucsd.edu)
[†]Senior authors: Sandipan Pati and Eric Halgren

Author contributions: C.W.D. and E.H. designed the study. E.T. and S.P. collected the data. C.D., I.A.V., S.K., and B.Q.R. analyzed the data. C.W.D. and E.H. wrote the manuscript. All authors reviewed and revised the manuscript. E.H. and S.P. supervised the work.

Competing interests: The authors declare no competing interests.

Acknowledgements: We thank Emília Tóth for helping with data collection. We also thank Adam Niese, Christopher Gonzalez, Daniel Cleary, and Jacob Garrett for their support. This work was supported by NIMH (1RF1MH117155-01, T32 MH020002) and ONR-MURI (N00014-16-1-2829).

Abstract

The co-occurrence of brief ~90 Hz oscillations (co-ripples) may be important in integrating information across the cortex and hippocampus, essential for sleep consolidation, and cognition in general. However, how such co-ripples are synchronized is unknown. We tested if cortico-cortical and hippocampal-cortical ripple co-occurrences are due to the simultaneous direct propagation of thalamic ripples, or if they are instead facilitated by lower frequency waves. Using human intracranial recordings, we found that ripples are generated in the thalamus during non-rapid eye movement sleep with similar characteristics as cortical and hippocampal ripples. However, thalamic ripples only infrequently and weakly co-occur, and never phase-lock, with cortical and hippocampal ripples. In contrast, thalamo-cortical spindles and upstates strongly facilitated cortico-cortical and hippocampo-cortical co-rippling. Thus, while thalamic ripples may not directly drive multiple cortical or hippocampal sites at ripple frequency, these sites may ripple synchronously in response to widespread activation from thalamo-cortical spindles and upstates.

Introduction

Ripples are brief high-frequency oscillations of the local field potential (LFP). In the rodent hippocampus during non-rapid eye movement sleep (NREM), ripples mark the replay of spatiotemporal firing patterns that play a crucial role in the consolidation of declarative memories (Buzsáki, 2015; Ego-Stengel and Wilson, 2009; Maingret et al., 2016; Wilson and McNaughton, 1994). In humans, ~70 ms long 90 Hz ripples are generated in the cortex during both NREM and waking (Dickey et al., 2022a; Dickey et al., 2022b). Cortical ripples couple to cortical and hippocampal ripples preceding recall (Dickey et al., 2022b; Vaz et al., 2019), when they entrain the replay of neuron firing sequences established during encoding (Vaz et al., 2020).

Spindles are 10-16 Hz oscillations that occur during NREM and are important for memory consolidation (Adamantidis et al., 2019). They are generated through interactions of intrinsic currents and local circuits in the thalamus (Destexhe and Sejnowski, 2003; McCormick et al., 2015) and are projected to all cortical areas (Mak-McCully et al., 2017; Piantoni et al., 2017), often on the down-to-upstate transition (Gonzalez et al., 2018), timing that is important for memory consolidation (Klinzing et al., 2019). Downstates and upstates comprise the slow oscillation and K-complex of human NREM, where cortical neurons are silent during downstates and fire at near-waking levels during upstates (Cash et al., 2009; Csercsa et al., 2010). Recurrent thalamo-cortical projections support the initiation, synchronization, and termination of spindles and down-to-upstates (Contreras et al., 1996; Crunelli et al., 2018; Mak-McCully et al., 2017). Critical to a possible role in consolidation, human cortical ripples occur during spindles just prior to the upstate peak (Dickey et al., 2022a), and mark the replay of cell-firing encoding motor patterns learned in prior waking (Rubin et al., 2022). Furthermore, hippocampal ripples are coordinated with cortical ripples (Dickey et al., 2022b; Vaz et al., 2019; Vaz et al., 2020), spindles, downstates, and upstates (Jiang et al., 2019a; b).

Crucially, human cortical ripples co-occur and phase-lock across long distances in multiple lobes in both hemispheres (Dickey et al., 2022b). Neither co-occurrence nor phase-locking decreases with separation between rippling locations, implying either a network of densely connected coupled cortical oscillators, or a central subcortical structure that broadly triggers and synchronizes cortical ripples. The thalamus is a prime candidate for this role given its ability to modulate and synchronize spindles and down-to-upstates across widespread cortical areas. Thus, the thalamus could also coordinate ripples in the hippocampus and cortex, via its direct anatomical connections with both structures (Varela et al., 2014). Consolidation during NREM in

mice is enhanced by optogenetic stimulation of the thalamus that evokes cortical spindles co-occurring with cortical upstates and hippocampal sharpwave-ripples (Latchoumane et al., 2017). Thus, the thalamus could synchronize ripples, either directly by generating ripples itself and projecting them widely, or indirectly by projecting spindles or upstates which in turn evoke ripples in multiple cortical and hippocampal locations.

Ripples have not been previously studied in the human thalamus. We analyzed intracranial recordings from non-epileptogenic and non-lesioned thalamus obtained from patients with epilepsy during seizure focus localization to determine if physiological ripples occur in the human thalamus, and if so, to elucidate their characteristics and relationships with cortical and hippocampal ripples. We then tested if thalamic ripples co-occur and phase-lock with cortical or hippocampal ripples, as would be expected if thalamic ripples directly synchronize ripples in these regions. To determine if the thalamus might synchronize cortical ripples indirectly, we tested if co-rippling between cortical sites during cortical spindles or upstates was more common when the thalamus also produced a spindle or upstate. We found that although the human anterior thalamus generates typical ripples during NREM, they are only weakly related to cortical or hippocampal ripples. However, thalamo-cortical spindles and upstates greatly increased the probability of co-rippling between cortical sites. Thus, the thalamus does not appear to drive widespread cortical ripple networks directly, but may indirectly facilitate ripple co-occurrence by synchronously modulating cortical sites through the projection of thalamic spindles and upstates.

Results

Thalamic, cortical, and hippocampal ripple characteristics during NREM

We detected ripples in the thalamus, cortex, and hippocampus of 10 patients undergoing seizure focus localization with intracranial electrodes (Supp. Table 1). All channels included in the study were trans-gray matter bipolar derivations to suppress volume conduction. All thalamic and cortical channels were in non-lesioned, non-epileptogenic tissue. Electrodes were implanted in several anterior thalamic nuclei, projecting mainly to lateral, medial and orbital prefrontal cortices, and the cingulate gyrus (Supp. Table 1). Sleep staging was performed to select NREM. Only channels and epochs that did not contain frequent inter-ictal spikes or artifacts were included in the study. Ripples were detected using a previously described method (Dickey et al., 2022a; Dickey et al., 2022b), requiring at least 3 distinct oscillation cycles. Events were rejected if they contained possible interictal spikes or artifacts. We found that in addition to the cortex and hippocampus, ripples were generated in the human anterior thalamus during NREM (Fig.1A-B; Supp. Fig.1).

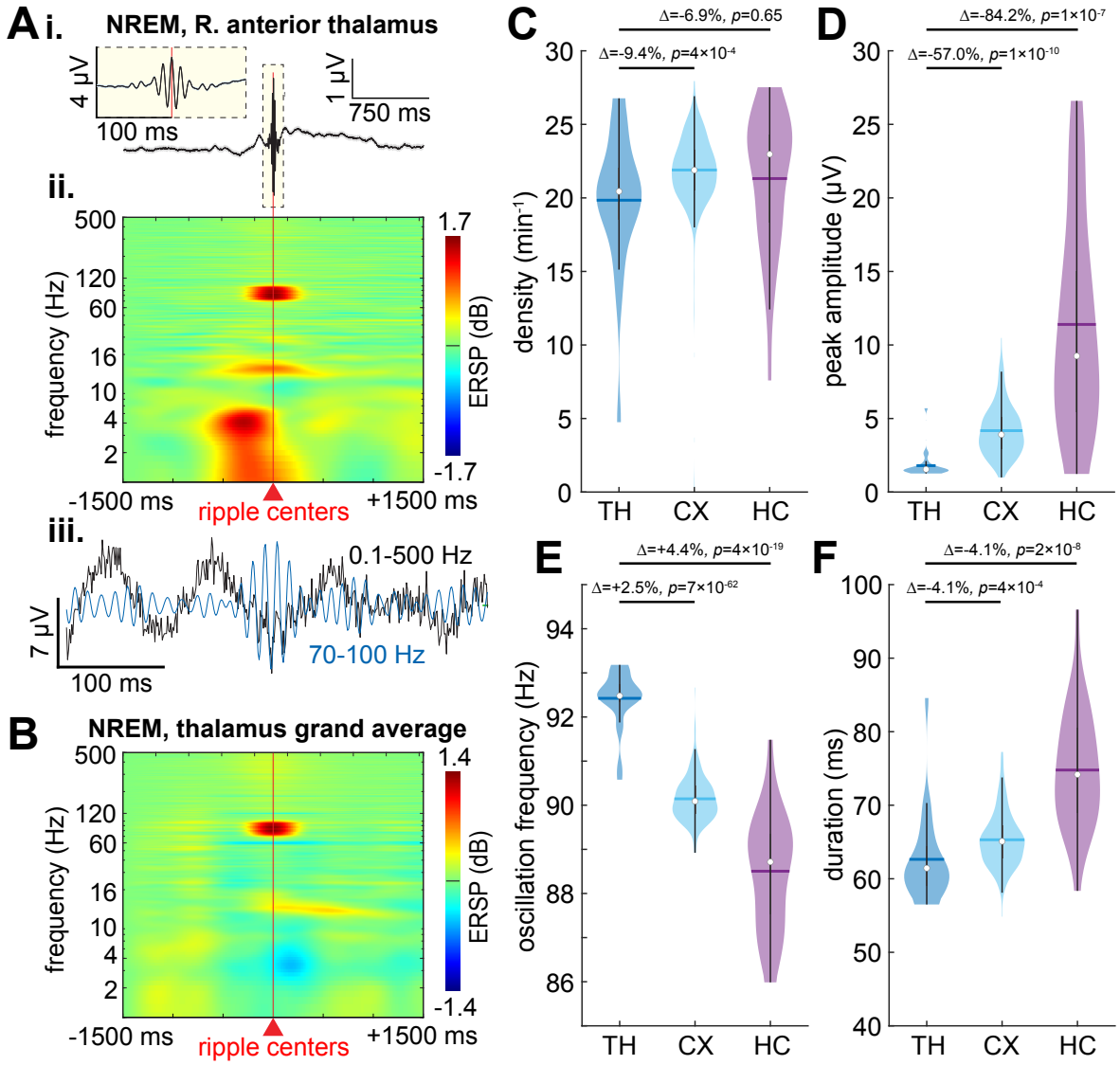

Figure 1. Ripples are generated in the human thalamus during NREM with similar characteristics as cortical and hippocampal ripples. (**A**) Ripples in one thalamic bipolar channel: (**i**) average broadband LFP, (**ii**) average time-frequency, and (**iii**) example single sweep broadband (black) and 70-100 Hz bandpass (blue). Shaded error shows SEM. In the time-frequency plot, note the focally increased power at ~90 Hz the time of increased 10-16 Hz spindle band activity, shortly following increased 0.1-4 Hz delta activity. In the single sweep, note the ripple occurrence on a ~12 Hz spindle. (**B**) Grand average time-frequency plot across the averages of all thalamic channels (N=24). (**C-F**) Thalamic, neocortical, and hippocampal ripple densities (**C**), peak 70-100 Hz analytic amplitudes (**D**), oscillation frequencies (**E**), and durations (**F**) across all channels (N_{TH}=24, N_{CX}=261, N_{HC}=31 channels from 10 patients) during NREM. Note the highly consistent densities of ~20 min^{-1}, oscillation frequencies of ~90 Hz, and durations of ~65 ms. Horizontal lines, means; circles, medians; vertical lines, interquartile ranges. Statistics performed with linear mixed-effects models with patient as random effect, and p-values are FDR-corrected for multiple comparisons across all channels from all patients. CT, computed tomography; CX, cortex; FDR, false discovery rate; HC, hippocampus; LFP, local field potential; MR, magnetic resonance; NREM, non-rapid eye movement sleep; SEM, standard error of the mean; TH, thalamus.

Thalamic ripples during NREM had a mean and standard deviation density (occurrence rate) of 19.8±4.6 min^{-1}, peak 70-100 Hz analytic amplitude of 1.79±0.91 μV, oscillation frequency of 92.4±0.63 Hz, and duration of 62.6±5.9 ms (Fig.1C-F; Supp. Table 2). Cortical ripples had an average density of 21.9±2.5 min^{-1}, amplitude of 4.17±1.69 μV, frequency of 90.1±0.5 Hz, and duration of 65.3±3.6 ms. Hippocampal ripples had an average density of 21.3±4.7 min^{-1}, amplitude of 11.39±7.23 μV, frequency of 88.5±1.3 Hz, and duration of 74.8±7.9 ms. See Fig.1C-F for statistical comparisons between thalamic and cortical or hippocampal characteristics. While thalamic ripples had smaller amplitudes than cortical or hippocampal ripples, they were easily distinguished from the baseline signal (Fig.1Aiii), which was also smaller. These characteristics were similar to those of hippocampal and cortical ripples, with the exception of hippocampal ripples having larger amplitudes (Fig.1C-F; Supp. Table 2). The relative sizes of ripples in thalamus, cortex, and hippocampus are consistent with the degree of lamination of neurons and synaptic inputs in the three structures, as well as previous observations that human ripples are larger in hippocampus than cortex (Dickey et al., 2022a), and that spindles and downstates are larger in cortex than thalamus (Mak-McCully et al., 2017).

Thalamic ripples are generated during thalamic spindles on the down-to-upstate transition

It is thought that the downstate is initiated in the cortex and then projects to the thalamus, where hyperpolarization releases h and T currents leading to the generation of a thalamic spindle that is then projected back to the cortex at the time of the down-to-upstate transition (Mak-McCully et al., 2017). This precisely timed sequence is important for memory consolidation. We found that, on average, thalamic ripples occur approximately 75 ms following thalamic downstate peaks (Fig.2A; N=9/24 channel pairs with significant modulations, post-FDR $p<0.05$, randomization test). Of the 9 channels with significant modulations, 4 had a significant sidedness preference, with all 4 showing downstates preceding ripples (post-FDR $p<0.05$, binomial test, expected value=0.5). Thalamic ripples tended to occur near thalamic spindle onsets (Fig.2B; N=7/24), and 0/7 channels with significant modulations had a significant sided preference. Thalamic ripples occurred about 250 ms preceding thalamic upstate peaks (Fig.2C; N=9/24). Of the 9 channels with significant modulations, all 9 had a significant sidedness preference, and 8 of the 9 showed thalamic ripples preceding thalamic upstate peaks.

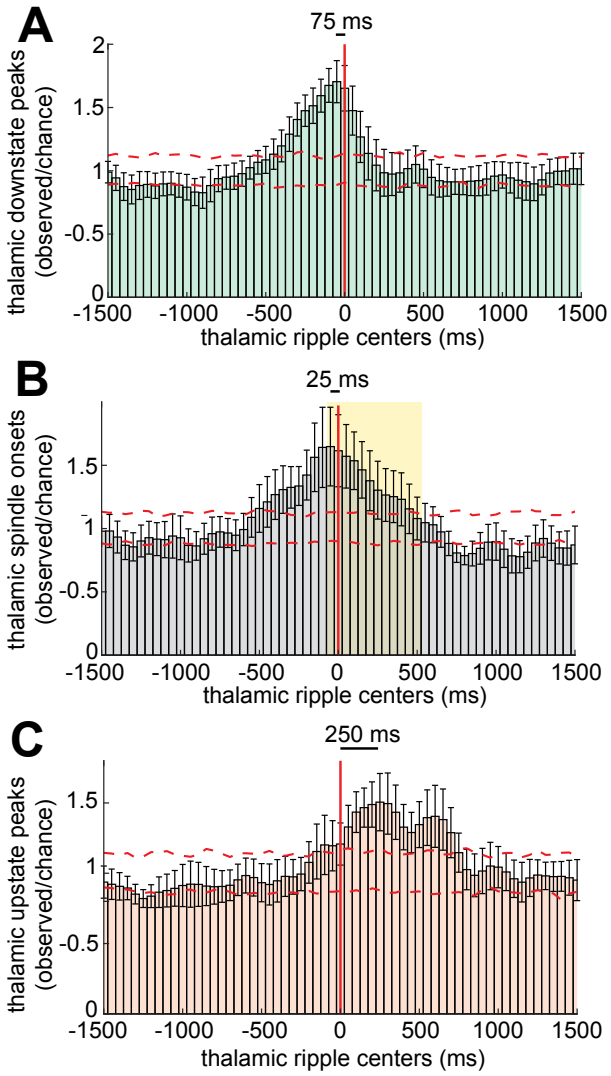

Figure 2. Thalamic ripples occur on the local down-to-upstate transition and near spindle onset, similar to cortical ripples. (**A**) Times of thalamic downstate peaks plotted relative to thalamic ripples at *t*=0 for channels that showed significant coupling (*N*=9/24 significant channels, post-FDR *p*<0.05, randomization test). (**B**) Times of thalamic spindle onsets relative to thalamic ripples (*N*=7/24). Shaded box denotes the average spindle interval. (**C**) Times of thalamic upstate peaks relative to thalamic ripples (*N*=9/24). Error bars show 99% confidence intervals.

Thalamic ripples weakly couple to and co-occur with cortical and hippocampal ripples

Previously, we showed that ripples frequently and strongly co-occur between cortical sites (i.e., cortico-cortical co-ripples) in widespread networks, and also between the hippocampus and cortex (i.e., hippocampo-cortical co-ripples) (Dickey et al., 2022b). One possible mechanism underlying this is a thalamo-cortical driving circuit. Therefore, we tested if thalamic ripples couple (within ±250 ms) or co-occur ('co-ripple'; ≥25 ms overlap) with cortical or hippocampal ripples. We found that thalamic ripples weakly couple with cortical (Fig.3A) and much less so hippocampal ripples (Fig.3B). By contrast, cortico-cortical (Fig.3C) and less so hippocampo-cortical (Fig.3D) sites had strongly coupled ripples. Cortico-cortical and hippocampo-cortical sites also were more

likely to co-ripple than thalamo-cortical and hippocampo-cortical (Fig.3E). Among thalamo-cortical channel pairs, only 14% (88/649) were significantly coupled (post-FDR $p<0.05$, randomization test) and 6% (40/649) had a significant number of co-occurrences above chance (post-FDR $p<0.05$, randomization test). Among thalamo-hippocampal pairs, even fewer, only 6% (5/81) were significantly coupled and 2% (2/81) had a significant number of co-occurrences. In contrast, among cortico-cortical pairs (including both orders for each pair), 54% (4174/7796) were significantly coupled and 47% (1828/3898) had a significant number of co-occurrences. Among hippocampo-cortical pairs, 51% (437/865) were significantly coupled and 15% (126/865) had significant co-occurrences. Thalamo-cortical co-ripple coupling was significantly less common than cortico-cortical ($p<0.00001$, $\chi^2=383.1$, df=1) or hippocampo-cortical ($p<0.00001$, $\chi^2=88.1$, df=1), which was also the case for co-occurrences (thalamo-cortical vs. cortico-cortical: $p<0.00001$, $\chi^2=381.4$, df=1; thalamo-cortical vs. hippocampo-cortical: $p<0.00001$, $\chi^2=26.8$, df=1). Across these 4 types of region pairs, the proportion of channel pairs with significant ripple coupling was significantly different ($p<0.00001$, $\chi^2=438.73$, df=3), as was the proportion of channel pairs with significant numbers of ripple co-occurrences above chance ($p<0.00001$, $\chi^2=485.3$, df=3).

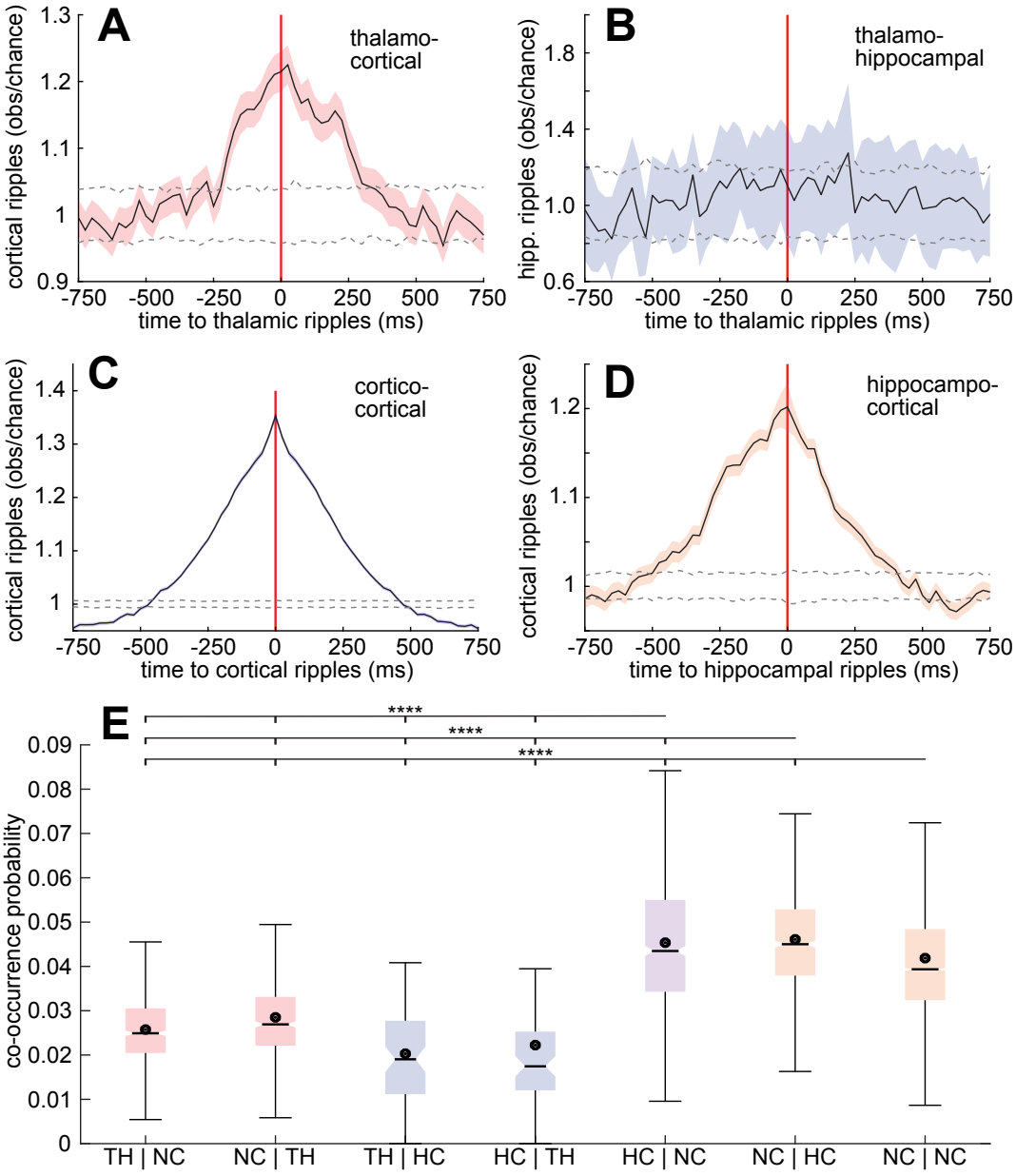

Figure 3. Thalamic ripples infrequently and weakly co-occur with cortical and hippocampal ripples during NREM. (**A**) Observed over chance occurrences of cortical ripples relative to thalamic ripples at t=0 (N=88/649 significant, post-FDR p<0.05, randomization test). Average across all significant channel pairs (25 ms Gaussian smoothed with σ=5 ms). Times of occurrences are ripple centers. (**B**) Same as (A) except hippocampal ripples relative to thalamic ripples (N=5/81). (**C**) Same as (A) except cortical ripples in one channel relative to cortical ripples in another channel (N=4174/7796). Note that no cortical bipolar channels included shared a common contact. (**D**) Same as (A) except hippocampal ripples relative to cortical ripples (N=437/865). (**E**) Conditional probabilities of ripple co-occurrences (≥25 ms overlap) between channels (e.g., TH | NC=probability of a thalamic ripple co-occurring with a given neocortical ripple). ****post-FDR p<0.0001, two-sided two-sample t-test. Shaded errors show 99% confidence intervals of the null distribution. Error bars show SEM.

Thalamic ripples do not phase-lock with cortical or hippocampal ripples

We previously showed that cortico-cortical but not hippocampo-cortical co-ripples often strongly phase-lock, suggesting a possible intracortical mechanism (Dickey et al., 2022b), however it is also possible that phase-locking between cortical locations is driven by a common input from thalamic ripples. To determine if channel pairs had phase-locked ripples, we computed phase-locking values (PLVs) (Lachaux et al., 1999), which measure phase consistency independent of amplitude, here using the 70-100 Hz phase across co-occurring ripples (≥25 ms overlap) at each time point for each channel pair (≥40 co-ripples required per pair). We found only one thalamo-cortical site pair had significantly phase-locked co-ripples (Supp. Fig.2A; N=1/451 significant channel pairs, post-FDR $p<0.05$, randomization test), and no thalamo-hippocampal site pairs had significantly phase-locked co-ripples (Supp. Fig.2B). Consistent with our previous results, cortico-cortical pairs had significantly phase-locked co-ripples (Supp. Fig.2C; N=52/2833), specifically about 8x as many as thalamo-cortical pairs, and no hippocampo-cortical pairs had phase-locked co-ripples (Supp. Fig.2D; N=0/490). Across these 4 types of region pairs, the proportion of phase-locked channel pairs was significantly different (p=0.001, χ^2=16.2, df=3). Thus, these results support our hypothesis that networks of phase-locked cortico-cortical co-ripples are directly driven intracortically rather than from thalamic or hippocampal inputs.

Thalamic spindles phase-lock with anterior cortical spindles

Given that cortical ripples occur during cortical spindles and phase-lock between cortical sites and between the cortex and hippocampus, we hypothesized that the thalamus organizes these networks by projecting spindles and upstates to the cortex. To test this hypothesis, we first computed 10-16 Hz PLVs between spindles in the thalamus and cortex. Since the anterior thalamus has more projections to the anterior than posterior cortex, we analyzed these regions separately (Fig.4A). In our analysis, the anterior cortex included orbitofrontal, prefrontal, and cingulate cortices, whereas the posterior cortex included all other cortical areas. We found significant thalamo-cortical spindle PLV modulations in the anterior cortex (Fig.4B; N=188/369 significant pairs, post-FDR $p<0.05$, randomization test) as well as the posterior cortex (Fig.4B; N=71/280). However, there was a significantly greater proportion of significant thalamo-cortical channel pairs in the anterior compared to posterior cortex ($p<0.00001$, χ^2=43.5, df=1). Furthermore, there was a greater mean PLV modulation amplitude within ±250 ms around the thalamo-cortical temporal centers in the anterior compared to posterior cortex ($p=5\times10^{-15}$, t=7.9, df=613, one-sided two-sample t-test). Results by individual cortical parcel are shown in Supp. Fig.3 These results are consistent with preferential projections of the anterior thalamus to the anterior cortex.

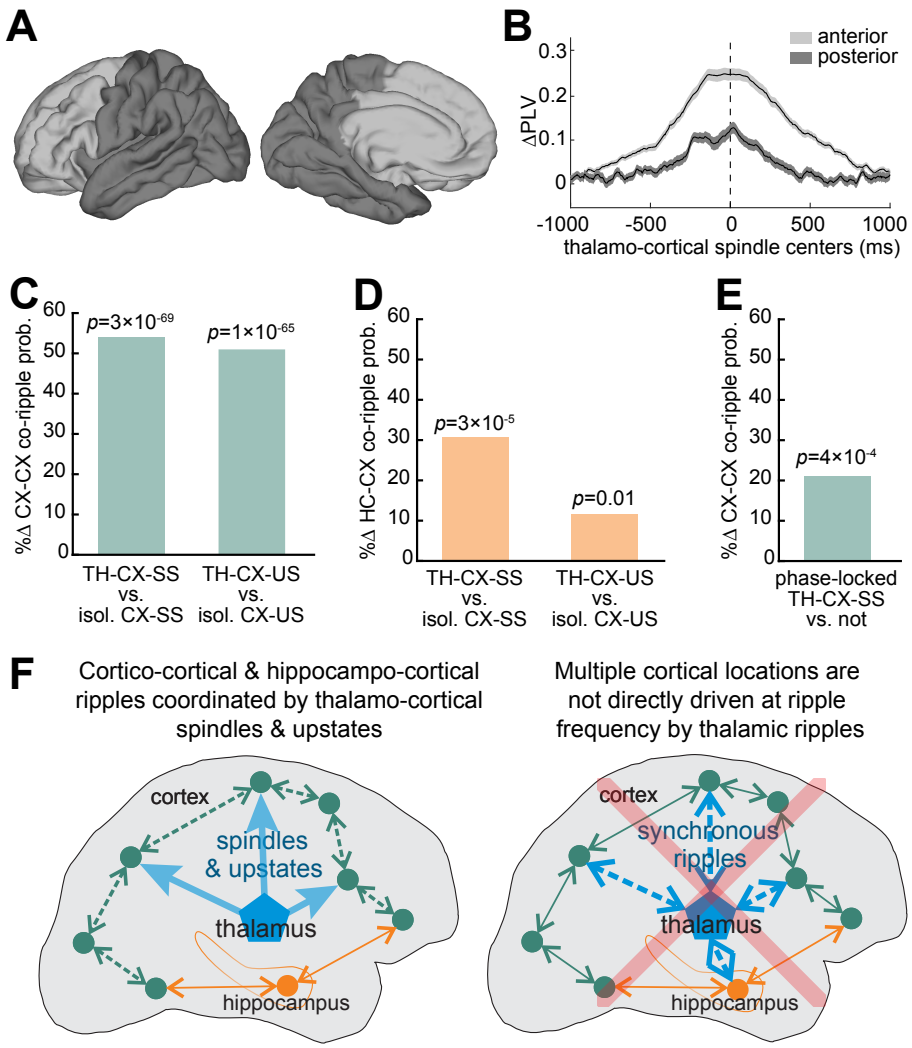

Figure 4. Thalamo-cortical spindles and upstates strongly enhance cortico-cortical and hippocampo-cortical co-rippling. (**A**) Division of the cortex into anterior and posterior regions based on connectivity with the anterior thalamus (anterior > posterior cortex). (**B**) Mean and standard deviation 10-16 Hz PLVs of thalamo-cortical spindles across significant thalamo-cortical channel pairs for anterior cortex (N=188/369 significant, post-FDR p<0.05, randomization test) compared to posterior cortex (N=71/280). Note the anterior cortex has a greater proportion of significant channels with greater phase-locking amplitudes. See Supp. Fig.3 for results by cortical parcel. (**C**) Mean percent increase in cortico-cortical co-ripple probability across cortico-cortical channel pairs when the thalamus is spindling with either cortical channel versus when it is not (left bar; one-sided paired t-test), and similar increase when thalamus and cortex share upstates versus when they do not (right). (**D**) Same as (C) except hippocampo-cortical co-ripple probability for isolated cortical vs. overlapping thalamo-cortical spindles or upstates. (**E**) Same as (C) except cortico-cortical co-ripple probability when one versus neither cortical channel has 10-16 Hz phase-locked spindles with the thalamus. (**F**) Proposed synergistic mechanisms (left) for achieving widely distributed cortical ripples that co-occur and phase-lock. Cortical depolarization via thalamo-cortical spindles and upstates (blue) trigger ripples which phase-lock through cortico-cortical coupling (green), and co-occur with hippocampal ripples via direct connections (orange). Our data do not support the alternative hypothesis (right) wherein thalamic ripples directly drive cortical and/or hippocampal ripples.

Projecting thalamo-cortical spindles and upstates organize cortico-cortical and hippocampo-cortical co-ripples

Because the data presented above does not support direct driving of cortical ripple co-occurrence by thalamic or hippocampal ripples, we hypothesized that they may be organized by interactions of slower waves, onto which ripples occur. In support of this hypothesis, we found that the probability of a cortico-cortical co-ripple occurring during a cortical spindle (on either channel) was significantly increased by 53% when there was a co-occurring thalamic spindle (on any channel) (Fig.4C; p=3×10^{-69}, t=18.0, N=2915 channel pairs from 10 patients, one-sided paired t-test). Furthermore, the probability of a cortico-cortical co-ripple preceding a cortical upstate peak (within 500 ms) was significantly increased by 51% when there was a preceding thalamic upstate peak (within 500 ms from the cortical upstate peak) (Fig.4C; p=1×10^{-65}, t=17.5, N=2942). Thus, these data indicate that projecting thalamic spindles and upstates (but not ripples) help to facilitate cortico-cortical co-ripples (Fig.4F).

In performing these same analyses except with respect to hippocampo-cortical co-ripples, the probability of a hippocampo-cortical co-ripple was significantly increased by 31% during thalamo-cortical versus isolated cortical spindles (Fig.4D; p=3×10^{-5}, t=4.0 N=544 channel pairs from 9 patients*)*, and significantly by 11% preceding a cortical upstate that was preceded by a thalamic upstate (Fig.4D; p=0.01, t=2.2, N=517*)*. Thus, projecting thalamic spindles and upstates appear to facilitate hippocampo-cortical in addition to cortico-cortical co-ripples (Fig.4F).

Phase-locked thalamo-cortical spindles facilitate cortico-cortical co-ripples

We showed that if a cortical site spindles with the thalamus during a ripple, it is more likely to co-ripple with another cortical site. We also found that thalamic spindles phase-lock with cortical spindles, consistent with a thalamo-cortical projection of spindles. We thus hypothesized that cortico-cortical co-rippling is driven by phase-locked thalamo-cortical spindles. We tested if cortico-cortical co-ripple probability is greater between cortical sites that have versus do not have 10-16 Hz spindles phase-locked with the thalamus. We found an increased cortico-cortical co-ripple probability when one versus neither cortical site had phase-locked spindles with the thalamus (Fig.4E; p=4×10^{-4}, t=3.3, df=1937). Thus, our data indicate that propagating phase-locked thalamo-cortical spindles drive networks of cortico-cortical co-ripples (Fig.4F).

Discussion

Previous work has shown that human cortical ripples often co-occur and even phase-lock at long separations, posing the question as to whether they are synchronized by a subcortical input (Dickey et al., 2022b). The present study investigates if ripples also occur in the human thalamus, and if so whether they, or other thalamic waves, have properties consistent with a role in synchronizing cortical ripples. Indeed, we found that ripples are generated in the human thalamus during NREM, with a similar oscillation frequency, occurrence density, and duration as cortical and hippocampal ripples. The oscillation frequency of thalamic ripples we found was ~90 Hz, which is similar to cortical (Dickey et al., 2022a; Dickey et al., 2022b) and hippocampal ripples (Jiang et al., 2019a; b) in humans, but lower than the 140-160 Hz ripples in rodents (Buzsáki, 2015). We found that, like cortical ripples (Dickey et al., 2022a), thalamic ripples tend to occur after the downstate, and just before the subsequent upstate peak, at the onset of the local sleep spindle.

Thalamic gamma, usually at 40 Hz but extending to 80 Hz, was previously recorded in cats and rodents, where it is generated by voltage-gated dendritic Ca^{2+} currents (Pedroarena and Llinás,

1997). This rhythmic firing led to the proposal that the thalamus drives synchronous gamma oscillations across widespread neocortical areas via the wide distribution of thalamo-cortical projections of the matrix system (Barth and MacDonald, 1996; Jones, 2009; Pedroarena and Llinás, 1997) (Jones, 2009; Llinás and Steriade, 2006), but direct evidence is absent.

A direct driving of cortical ripples by thalamic ripples would imply a high level of synchrony between them. However, we found that thalamic ripples only very rarely and weakly co-occur or phase-lock with cortical ripples. These findings, in stark contrast to the robust co-occurrence of cortical ripples with other cortical sites in this and our previous study (Dickey et al., 2022b), suggest that thalamic ripples have minimal or no direct role in driving widespread forebrain ripple synchrony.

Although cortical ripples did not synchronize with thalamic ripples, cortico-cortical co-rippling was strongly promoted by the co-occurrence of sleep spindles or upstates in the thalamus and cortex. Critically, when either spindles or upstates coincide between the thalamus and a cortical site, we found that the cortical site is ~40-50% more likely to co-ripple with another cortical site. We also found that thalamic spindles can phase-lock with cortical, preferentially in the anterior cortex, which is consistent with anatomical projections from the anterior thalamus. We found that thalamo-cortical spindle phase-locking further enhances cortical co-rippling. Thus, it appears that the thalamus does help to coordinate cortical co-rippling, not by projecting ripples to multiple cortical locations, but by modulating multiple cortical areas by projecting spindles and upstates. This is consistent with the previously observed functional coupling between thalamic and cortical spindles and down-to-upstates in humans (Mak-McCully et al., 2017) and animals (Contreras et al., 1996; Crunelli et al., 2018).

The mechanism whereby thalamic spindles and upstates may help trigger cortical ripples could be through depolarizing cortical neurons for ~50-100 ms. Evidence for such depolarizations during NREM has been found in the prominent current sinks and large increases in both pyramidal and interneuron firing in microelectrode array recordings from human cortex during upstates and spindles (Cash et al., 2009; Csercsa et al., 2010; Dickey et al., 2022a; Hagler et al., 2018). Rodent hippocampal ripples can be induced by such broad ~60 ms duration depolarizing pulses, via a mechanism involving pyramidal-basket cell feedback loops ('PING') synchronized by basket–basket cell co-firing ('ING') (Stark et al., 2014). Further evidence that this mechanism is engaged in human cortical ripples during NREM is that they are accompanied by large increases in firing phase-locked to ripple oscillations, with pyramidal cells leading interneurons (Dickey et al., 2022a).

We also examined the three-way relationships among thalamic, hippocampal, and cortical ripples. We found that thalamic ripples only very rarely and weakly co-occur and do not phase-lock with hippocampal ripples. We also confirmed our previous finding that cortical ripples do not phase-lock with hippocampal ripples but co-occur at a moderate rate (Dickey et al., 2022b). Thus, we found no evidence that hippocampal ripples are driven by thalamic ripples, or that they directly drive cortical ripples. However, since hippocampal ripples are coordinated with cortical spindles, downstates, and upstates (Jiang et al., 2019a; b), the thalamus could also coordinate ripples in both the hippocampus and cortex, via a depolarizing modulation as outlined above, rather than via high-frequency oscillatory driving. Indeed, we found that thalamic upstates that project to the cortex or hippocampus were associated with an increased probability of hippocampo-cortical co-ripples. Thus, our results support a role of slower thalamic waves in organizing hippocampo-cortico-cortical networks of co-occurring ripples.

Overall, our findings are consistent with cortico-cortical ripple synchrony arising from direct interactions between cortical neurons. Cortico-cortical ripple synchrony has been proposed to support binding of the information encoded in the interacting locations (Dickey et al., 2022b; Gray et al., 1989). In such models, oscillations not only modulate the interaction of cortical areas through phase-selection (Fries, 2009) and coincidence detection (Salinas and Sejnowski, 2001), these interactions themselves reinforce the oscillations through re-entrance (Bazhenov et al., 2008; Vicente et al., 2008). A mutually-reinforcing mechanism is consistent with our previous finding of a strong dependence of phase-locking on the co-rippling of several cortical locations simultaneously, beyond the two whose ripple phase-locking is being measured (Dickey et al., 2022b). Since integration of specific information requires a high bandwidth, it could only be transmitted by direct cortico-cortical connections in humans, given that neuroanatomical calculations find that >95% of synapses on cortical cells are from the cortex (reviewed in Rosen and Halgren (2022)). In particular, the ratio of cortical neurons to thalamo-cortical projection cells is ~1400:1 (calculations based on human thalamic cell counts in Xuereb et al. (1991), proportion of thalamo-cortical cells in Arcelli et al. (1997), and cortical cell counts in Azevedo et al. (2009)). Thus, phase-locking arising from cortico-cortical interactions is consistent with the proposed role of co-ripples in supporting cross-cortical information binding. Our finding that thalamo-cortical spindles and upstates, but not thalamic ripples, enhance cortico-cortical and hippocampo-cortical co-rippling is consistent with the thalamus having a modulatory rather than high-frequency driving role in promoting co-rippling.

In sum, we provide the first evidence that ripples are generated in the human thalamus and have similar characteristics as hippocampal and cortical ripples. Due to infrequent and weak co-occurrence and phase-locking between ripples in the thalamus and those in the cortex or hippocampus, it is unlikely that thalamic ripples directly drive cortico-cortical or hippocampal-cortical ripple co-occurrence or phase-locking. Rather, we found evidence that thalamic upstates, spindles, and especially phase-locked spindles facilitate the co-occurrence of ripples in the cortex. This may help to organize replay that underlies the consolidation of memories across widespread areas in the cortex.

Methods

Patient selection, intracranial recordings, and data pre-processing

Data from 10 patients (5 female, 40.9±11.4 years old) with pharmaco-resistant focal epilepsy undergoing intracranial recording for approximately one to two weeks to localize seizure onset zones prior to surgical resection were included in this study (Supp. Table 1). Implantation and consent procedures have been described (Chaitanya et al., 2020). Patients were only included in this study if they had no prior brain surgery and normal background LFPs except for infrequent epileptiform activity. A total of 14 patients with thalamic electrodes were rejected due to abnormal LFPs. Recordings were collected with a Natus Quantum amplifier at 2048 Hz sampling with a 0.016-683 Hz bandpass. PMT Electrodes were 0.8 mm diameter with 10-16 2 mm long contacts at 3.5-5 mm pitch (~150 contacts/patient). Data preprocessing was performed in Matlab 2019b and LFPs were inspected visually using the Fieldtrip toolbox (Oostenveld et al., 2011). Data were downsampled to 1000 Hz, with anti-aliasing at 500 Hz, and notch filtered at 60 Hz with 60 Hz harmonics up to 480 Hz.

Channel selection

Channels were bipolar derivations of adjacent contacts to ensure measurement of LFPs. Channels were only included if their contacts were in non-epileptogenic, non-lesioned thalamus

as well as cortex, and in 9 of the 10 patients also hippocampus. Channels were manually selected based on NREM averages of delta (0.5-2 Hz) and high-gamma (70-190 Hz) analytic amplitudes. Generally, cortical channels selected had an average delta analytic amplitude greater than 40 μV, hippocampal channels had a delta amplitude greater than 15 μV, and thalamic channels had a delta amplitude greater than 5 μV. Channels were then visually inspected during NREM periods to ensure they did not have frequent interictal spikes or artifacts and had a normal appearing broadband signal. Among 1845 bipolar channels (1157 left sided) across the patients in the study, a total of 316 (110 left sided) were included in the study. From a total of 30 thalamic bipolar channels across the patients in the study, 24 were included in the study because they had normal appearing LFPs without evidence of frequent inter-ictal spiking. Note that the majority of channels were excluded because they were not in thalamic, cortical, or hippocampal gray matter, and thus would not record meaningful local neuronal activity. Furthermore, cortical and hippocampal channels were excluded if they shared a common contact with another bipolar channel that was included in the analysis.

Channel localization

Cortical surfaces were reconstructed using the pre-operative T1-weighted structural MR volume with the FreeSurfer recon-all pipeline (Fischl, 2012). Atlas-based automated parcellation (Fischl et al., 2004) was utilized to assign anatomical labels to cortical surface regions according to the Destrieux et al. (2010) atlas, and subsequently amalgamated into cortical parcels per Desikan et al. (2006). For analyses involving anterior versus posterior cortex, anterior cortex included Desikan parcels that comprise the orbitofrontal cortex (frontal pole, lateral orbitofrontal, medial orbitofrontal, pars orbitalis), prefrontal cortex (caudal middle frontal, pars opercularis, pars triangularis, rostral middle frontal, superior frontal), and cingulate cortex (caudal anterior cingulate, rostral anterior cingulate, posterior cingulate). Posterior cortex was comprised of the remaining cortical parcels.

To localize the SEEG contacts, the post-implant CT volume was co-registered to the pre-implant MR volume in standardized 1mm isotropic FreeSurfer space with the general registration module (Johnson et al., 2007) in 3D Slicer (Fedorov et al., 2012). Next, each contact's position in FreeSurfer coordinates was determined by manually marking the contact centroid as visualized in the co-registered CT volume. Each transcortical bipolar channel was assigned an anatomical parcel from the above atlas through determining the parcel identities of the white-gray surface vertex nearest to the midpoint of the adjacent contacts. Automated segmentation assigned a nucleus to each voxel of the MR volume in the thalamus (Iglesias et al., 2018), which was confirmed by visual comparison with the Allen Brain Atlas (https://atlas.brain-map.org/). The 24 thalamic bipolar channels included the following nuclei (in descending frequency): AnteroVentral, Ventral Anterior, Reticular, Ventral Lateral, Fasciculus, MedioDorsal, and CentroMedian (Supp. Table 1). Due to possible inaccuracies in registration and limitations of visible nuclear boundaries, assignment of contacts to particular nuclei should be considered approximate. Transcortical bipolar locations were registered to the fsaverage template brain for visualization through spherical morphing (Fischl et al., 1999). All contacts marked as thalamic or hippocampal were confirmed to localize to these respective structures through visual inspection of the co-registered pre-operative MRI and post-operative CT.

Sleep staging and epoch selection

Sleep staging was performed to select NREM stages N2 and N3 consistent with Silber et al. (2007). Data were bandpassed at 0.5-2 Hz and then Hilbert transformed to obtain the delta analytic amplitudes. NREM epochs were selected for analysis when the cortical channels had

increased delta analytic amplitude during overnight hours (8:00 PM-8:00 AM). These epochs subsequently underwent visual confirmation that they contained frequent and prominent slow wave oscillations and spindles characteristic of NREM stages N2 and N3 sleep. Epochs were only retained when they were absent of frequent inter-ictal spikes or artifacts.

Time-frequency analyses

Time-frequency plots of ripple-triggered spectral power were generated from the broadband LFP using EEGLAB (Delorme and Makeig, 2004). Power was calculated from 1-500 Hz by averaging the fast Fourier transforms with Hanning window tapering locked to the centers of 5000 randomly sub-selected ripples per channel. Each 1 Hz frequency bin was normalized to the mean power at -2 to -1.5 s and then masked with two-tailed bootstrapped significance (N=200 shuffles) with p-values FDR-corrected with α=0.05 using a -2 to -1.5 s baseline. Grand average time-frequency plots were produced by averaging across the channel average time-frequency plots.

Ripple detection

Ripples were detected in the thalamus, cortex, and hippocampus based on previously published methods (Dickey et al., 2022a; Dickey et al., 2022b). For each channel, data were bandpassed at 70-100 Hz with a 6th order forward-reverse Butterworth filter (zero-phase shift) and peaks in the analytic amplitude of the Hilbert transform were selected if they were at least 3 standard deviations above the channel mean. Event onsets and offsets were found on both sides of the peak when the 70-100 Hz analytic amplitude decreased below a z-score of 0.75. Events were retained if they had at least 3 oscillation peaks in the 120 Hz lowpass, determined by moving a 40 ms window in 5 ms increments ±50 ms relative to the midpoint of the ripple, requiring at least 1 window to have at least 3 peaks. Adjacent events within 25 ms were merged and ripple centers were determined as the time of the largest positive peak in the 70-100 Hz bandpass.

To exclude epileptiform activity and artifacts, events were rejected when the absolute value of the z-score of the 100 Hz highpass was greater than 7. Events were also rejected if they were within ±500 ms from putative interictal spikes (detection criteria described below). Furthermore, events were rejected if they coincided with a putative interictal spike detected on any channel to exclude events that could be coupled across channels due to epileptiform activity. Lastly, events were rejected if the largest peak-to-valley or valley-to-peak absolute amplitude in the broadband LFP was 2.5 times greater than the third largest in order to exclude events that had only one prominent cycle or deflection. The average broadband LFP and average time-frequency plots locked to ripple centers as well as multiple individual broadband LFP ripples were visually examined in each channel from each patient to confirm there were multiple distinct cycles in the 70-100 Hz band, without contamination by possible artifacts or epileptiform transients. The oscillation frequency of each ripple was computed as follows:

$$f = \frac{N}{2 \times d} \tag{1}$$

Where N is the number of 70-100 Hz zero crossings (i.e., half cycles, with fractional cycles determined based on the remaining phase angle over π), and d is the duration of the ripple.

Interictal spike rejection

Ripples were excluded from analysis if they were within 500 ms from putative interictal spikes. Putative interictal spikes were detected by finding a high frequency score, which was the 20 ms

boxcar smoothed 70-190 Hz analytic amplitude, and a spike template score, which was computed as the cross-covariance with a template interictal spike. A putative interictal spike was marked when the sum of the high frequency score, weighted by 13, and the spike template score, weighted by 25, exceeded 130. These thresholds were determined through extensive visual examination of many hundreds of events across multiple channels from multiple patients.

Downstate, upstate, and spindle detection

Downstates and upstates were detected according to previously published methods (Dickey et al., 2021; Dickey et al., 2022a; Jiang et al., 2019a; b). Data were bandpassed from 0.1-4 Hz and the top 10% of amplitude peaks between consecutive zero crossings within 0.25-3 s were identified. The polarity of each signal was inverted if needed so that downstates were negative and upstates were positive. This was done by confirming that the average 70-190 Hz analytic amplitude ±100 ms around peaks was greater for upstates than downstates for each channel.

Spindles were also detected according to a previously published method (Dickey et al., 2021; Dickey et al., 2022a; Hagler et al., 2018). Data were bandpassed at 10-16 Hz, and the absolute values were smoothed with convolution using a tapered 300 ms Tukey window, then median values were subtracted from each channel. Data were normalized by the median absolute deviation, and spindles were identified when peaks exceeded 1 for a minimum of 400 ms. Onsets and offsets were marked when these amplitudes fell below 1. Putative spindles coinciding with large increases in lower (4-8 Hz) or higher (18-25 Hz) power were rejected to exclude broadband events and theta bursts, which may overlap with slower spindle frequencies (Gonzalez et al., 2018).

Ripple timing and co-occurrence analyses

Timing relationships between ripples and other sleep waves were computed as previously described (Dickey et al., 2022a). Times of ripple centers relative to spindle onsets, downstate peaks, and upstate peaks on the same channel were determined for each channel. Event counts were calculated in 50 ms bins ±1500 ms around cortical ripple centers. Time histogram plots were smoothed with a 50 ms Gaussian window with σ=10 ms.

Cortical ripples were considered to co-occur ('co-ripple') if they overlapped for at least 25 ms in two different cortical bipolar channels (no cortical bipolar channels shared a common contact). A cortical co-ripple was determined to co-occur with an isolated cortical spindle if its time center occurred during a spindle on either cortical channel without a thalamic spindle onset preceding the cortical spindle onset within 500 ms on any thalamic channel. A cortical co-ripple was determined to co-occur with a thalamo-cortical spindle if there was a thalamic spindle on any thalamic channel with an onset within 500 ms preceding the cortical spindle onset. Probabilities were computed as the number of co-ripples divided by the total time of cortical spindling, including only the cortical spindles selected for each condition as described above. This same method was used to compute the probability that a cortical co-ripple occurred within 500 ms preceding isolated cortical upstates compared to thalamo-cortical upstates, where the thalamic upstate peak preceded the cortical upstate peak within 500 ms. Channel pairs were excluded from statistical analysis if there were no co-ripples in either condition being compared or if there was less than 15 s of total cortical spindling time.

Phase-locking analyses

Phase-locking of co-occurring ripples/spindles at different sites was evaluated using the phase-locking value (PLV), which is an instantaneous measure of phase consistency that is independent of signal amplitudes (Lachaux et al., 1999). PLV time courses were determined using the analytic angles of the 70-100 Hz (for ripples) or 10-16 Hz (for spindles) bandpass (6th order zero-phase shift forward-reverse filtered) of each channel pair when there were at least 40 co-ripples that overlapped for at least 25 ms or 40 co-spindles that overlapped for at least 200 ms. PLVs were computed in 1 ms timesteps relative to the temporal centers of the co-ripples/spindles. A null distribution was generated by randomly selecting 200 times within -10 to -2 s preceding each co-ripple/spindle center. Pre-FDR *p*-values were computed by comparing the observed vs. null distributions in 5 ms bins within ±50 ms around the co-ripple centers or within 50 ms bins within ±250 ms around the co-spindle centers. *P*-values were then FDR-corrected across bins and channel pairs. A channel pair was determined to have significant ripple phase-locking if at least 2 consecutive bins had post-FDR $p<0.05$. PLV plots were Gaussian smoothed with a window of 10 ms and $\sigma=2$ ms.

Experimental design and statistical analyses

Statistical analyses were performed with $\alpha=0.05$ and all *p*-values involving multiple comparisons were FDR-corrected across all channels from all patients unless specified otherwise. Random shuffling statistics were performed with $N=200$ iterations per channel or channel pair. Paired and two-sample *t*-tests were used to compare distribution means. To determine if a peri-event time histogram was significant for a given channel or channel pair, a null distribution was found by shuffling the events relative to the ripples within ±1.5 s 200 times per channel pair or channel. *P*-values were computed by a comparison of the observed and null distributions for each bin over ±25 ms for ripples or ±50 ms (250 ms Gaussian smoothed with $\sigma=50$ ms) for other sleep waves. These *p*-values were then FDR-corrected across all bins across all channels/channel pairs. A channel/channel pair had a significant modulation if 3 or more consecutive bins had post-FDR $p<0.05$. Whether a given channel/channel pair had a leading/lagging relationship between events was determined using a two-sided binomial test to compare the counts in the 250 ms preceding vs. following $t=0$ with an expected value of 0.5. Whether a channel pair had significantly greater co-rippling compared to chance was determined by randomly shuffling ($N=200$ iterations) the inter-ripple ripple intervals in moving non-overlapping 5 min windows on each channel and comparing the observed vs. null number of co-occurrences. These *p*-values were FDR-corrected across all channel pairs. Comparisons of proportions (e.g., proportions of significant channel pairs for various conditions) were performed with a χ^2 test of proportions.

To test for differences of ripple characteristics (i.e., density, amplitude, frequency, duration) between different regions, we used the following linear-mixed effects model formula to control for patient as a random effect, with subsequent FDR-correction for multiple comparisons (across all channels from all patients):

$$\textit{characteristic} \sim \textit{region} + (1 \mid \textit{patient}) \qquad (2)$$

Data availability

The de-identified raw data that support the findings of this study are available from the corresponding authors upon reasonable request provided that the data sharing agreement and patient consent permit that sharing.

Code availability

The code that support the findings of this study are available from the corresponding authors upon reasonable request.

References

Adamantidis, A.R., Gutierrez Herrera, C., and Gent, T.C. (2019). Oscillating circuitries in the sleeping brain. Nature Reviews Neuroscience *20*, 746-762. 10.1038/s41583-019-0223-4.

Arcelli, P., Frassoni, C., Regondi, M.C., De Biasi, S., and Spreafico, R. (1997). GABAergic neurons in mammalian thalamus: a marker of thalamic complexity? Brain Research Bulletin *42*, 27-37. 10.1016/s0361-9230(96)00107-4.

Azevedo, F.A., Carvalho, L.R., Grinberg, L.T., Farfel, J.M., Ferretti, R.E., Leite, R.E., Jacob Filho, W., Lent, R., and Herculano-Houzel, S. (2009). Equal numbers of neuronal and nonneuronal cells make the human brain an isometrically scaled-up primate brain. Journal of Comparative Neurology *513*, 532-541. 10.1002/cne.21974.

Barth, D.S., and MacDonald, K.D. (1996). Thalamic modulation of high-frequency oscillating potentials in auditory cortex. Nature *383*, 78-81. 10.1038/383078a0.

Bazhenov, M., Rulkov, N.F., and Timofeev, I. (2008). Effect of synaptic connectivity on long-range synchronization of fast cortical oscillations. Journal of Neurophysiology. 10.1152/jn.90613.2008.

Buzsáki, G. (2015). Hippocampal sharp wave-ripple: A cognitive biomarker for episodic memory and planning. Hippocampus *25*, 1073-1188. 10.1002/hipo.22488.

Cash, S.S., Halgren, E., Dehghani, N., Rossetti, A.O., Thesen, T., Wang, C., Devinsky, O., Kuzniecky, R., Doyle, W., Madsen, J.R., et al. (2009). The human K-complex represents an isolated cortical down-state. Science *324*, 1084-1087. 10.1126/science.1169626.

Chaitanya, G., Romeo, A.K., Ilyas, A., Irannejad, A., Toth, E., Elsayed, G., Bentley, J.N., Riley, K.O., and Pati, S. (2020). Robot-assisted stereoelectroencephalography exploration of the limbic thalamus in human focal epilepsy: implantation technique and complications in the first 24 patients. Neurosurg Focus *48*, E2. 10.3171/2020.1.Focus19887.

Contreras, D., Destexhe, A., Sejnowski, T.J., and Steriade, M. (1996). Control of spatiotemporal coherence of a thalamic oscillation by corticothalamic feedback. Science *274*, 771-774. 10.1126/science.274.5288.771.

Crunelli, V., Lőrincz, M.L., Connelly, W.M., David, F., Hughes, S.W., Lambert, R.C., Leresche, N., and Errington, A.C. (2018). Dual function of thalamic low-vigilance state oscillations: rhythm-regulation and plasticity. Nature Reviews Neuroscience *19*, 107. 10.1038/nrn.2017.151.

Csercsa, R., Dombovari, B., Fabo, D., Wittner, L., Eross, L., Entz, L., Solyom, A., Rasonyi, G., Szucs, A., Kelemen, A., et al. (2010). Laminar analysis of slow wave activity in humans. Brain *133*, 2814-2829. 10.1093/brain/awq169.

Delorme, A., and Makeig, S. (2004). EEGLAB: An open source toolbox for analysis of single-trial EEG dynamics including independent component analysis. Journal of Neuroscience Methods *134*, 9-21. 10.1016/j.jneumeth.2003.10.009.

Desikan, R.S., Segonne, F., Fischl, B., Quinn, B.T., Dickerson, B.C., Blacker, D., Buckner, R.L., Dale, A.M., Maguire, R.P., Hyman, B.T., et al. (2006). An automated labeling system for subdividing the human cerebral cortex on MRI scans into gyral based regions of interest. NeuroImage *31*, 968-980. 10.1016/j.neuroimage.2006.01.021.

Destexhe, A., and Sejnowski, T.J. (2003). Interactions between membrane conductances underlying thalamocortical slow-wave oscillations. Physiological Reviews *83*, 1401-1453. 10.1152/physrev.00012.2003.

Destrieux, C., Fischl, B., Dale, A., and Halgren, E. (2010). Automatic parcellation of human cortical gyri and sulci using standard anatomical nomenclature. Neuroimage *53*, 1-15. 10.1016/j.neuroimage.2010.06.010.

Dickey, C.W., Sargsyan, A., Madsen, J.R., Eskandar, E.N., Cash, S.S., and Halgren, E. (2021). Travelling spindles create necessary conditions for spike-timing-dependent plasticity in humans. Nature Communications *12*, 1027. 10.1038/s41467-021-21298-x.

Dickey, C.W., Verzhbinsky, I.A., Jiang, X., Rosen, B.Q., Kajfez, S., Eskandar, E.N., Gonzalez-Martinez, J., Cash, S.S., and Halgren, E. (2022a). Cortical ripples during NREM sleep and waking in humans. Journal of Neuroscience, JN-RM-0742-0722. 10.1523/jneurosci.0742-22.2022.

Dickey, C.W., Verzhbinsky, I.A., Jiang, X., Rosen, B.Q., Kajfez, S., Stedelin, B., Shih, J.J., Ben-Haim, S., Raslan, A.M., Eskandar, E.N., et al. (2022b). Widespread ripples synchronize human cortical activity during sleep, waking, and memory recall. Proceedings of the National Academy of Sciences *119*, e2107797119. 10.1073/pnas.2107797119.

Ego-Stengel, V., and Wilson, M.A. (2009). Disruption of ripple-associated hippocampal activity during rest impairs spatial learning in the rat. Hippocampus *20*, 1-10. 10.1002/hipo.20707.

Fedorov, A., Beichel, R., Kalpathy-Cramer, J., Finet, J., Fillion-Robin, J.C., Pujol, S., Bauer, C., Jennings, D., Fennessy, F., Sonka, M., et al. (2012). 3D Slicer as an image computing platform for the Quantitative Imaging Network. Magnetic Resonance Imaging *30*, 1323-1341. 10.1016/j.mri.2012.05.001.

Fischl, B. (2012). FreeSurfer. Neuroimage *62*, 774-781. 10.1016/j.neuroimage.2012.01.021.

Fischl, B., Sereno, M.I., Tootell, R.B., and Dale, A.M. (1999). High-resolution intersubject averaging and a coordinate system for the cortical surface. Hum Brain Mapp *8*, 272-284. 10.1002/(sici)1097-0193(1999)8:4<272::aid-hbm10>3.0.co;2-4.

Fischl, B., van der Kouwe, A., Destrieux, C., Halgren, E., Ségonne, F., Salat, D.H., Busa, E., Seidman, L.J., Goldstein, J., Kennedy, D., et al. (2004). Automatically parcellating the human cerebral cortex. Cereb Cortex *14*, 11-22. 10.1093/cercor/bhg087.

Fries, P. (2009). Neuronal gamma-band synchronization as a fundamental process in cortical computation. Annual Review of Neuroscience *32*, 209-224. 10.1146/annurev.neuro.051508.135603.

Gonzalez, C.E., Mak-McCully, R.A., Rosen, B.Q., Cash, S.S., Chauvel, P.Y., Bastuji, H., Rey, M., and Halgren, E. (2018). Theta bursts precede, and spindles follow, cortical and thalamic downstates in human NREM sleep. Journal of Neuroscience *38*, 9989-10001. 10.1523/jneurosci.0476-18.2018.

Gray, C., Konig, P., Engel, A., and Singer, W. (1989). Oscillatory responses in cat visual cortex exhibit inter-columnar synchronization which reflects global stimulus properties. Nature *338*, 334-337. 10.1038/338334a0.

Hagler, D.J., Ulbert, I., Wittner, L., Erőss, L., Madsen, J.R., Devinsky, O., Doyle, W., Fabo, D., Cash, S.S., and Halgren, E. (2018). Heterogeneous origins of human sleep spindles in different cortical layers. Journal of Neuroscience *38*, 3013-3025. 10.1523/jneurosci.2241-17.2018.

Iglesias, J.E., Insausti, R., Lerma-Usabiaga, G., Bocchetta, M., Van Leemput, K., Greve, D.N., van der Kouwe, A., Fischl, B., Caballero-Gaudes, C., and Paz-Alonso, P.M. (2018). A probabilistic atlas of the human thalamic nuclei combining ex vivo MRI and histology. NeuroImage *183*, 314-326. 10.1016/j.neuroimage.2018.08.012.

Jiang, X., Gonzalez-Martinez, J., and Halgren, E. (2019a). Coordination of human hippocampal sharpwave ripples during NREM sleep with cortical theta bursts, spindles, downstates, and upstates. Journal of Neuroscience *39*, 8744-8761. 10.1523/jneurosci.2857-18.2019.

Jiang, X., Gonzalez-Martinez, J., and Halgren, E. (2019b). Posterior hippocampal spindle-ripples co-occur with neocortical theta-bursts and down-upstates, and phase-lock with parietal spindles during NREM sleep in humans. Journal of Neuroscience, 2858-2818.

Johnson, H., Harris, G., and Williams, K. (2007). BRAINSFIT: Mutual information registrations of whole-brain 3D Images, using the insight toolkit.

Jones, E.G. (2009). Synchrony in the interconnected circuitry of the thalamus and cerebral cortex. Annals of the New York Academy of Sciences *1157*, 10-23. 10.1111/j.1749-6632.2009.04534.x.

Klinzing, J.G., Niethard, N., and Born, J. (2019). Mechanisms of systems memory consolidation during sleep. Nature Neuroscience *22*, 1598-1610. 10.1038/s41593-019-0467-3.

Lachaux, J.P., Rodriguez, E., Martinerie, J., and Varela, F.J. (1999). Measuring phase synchrony in brain signals. Human Brain Mapping *8*, 194-208.

Latchoumane, C.-F.V., Ngo, H.-V.V., Born, J., and Shin, H.-S. (2017). Thalamic spindles promote memory formation during sleep through triple phase-locking of cortical, thalamic, and hippocampal rhythms. Neuron *95*, 424-435.e426. 10.1016/j.neuron.2017.06.025.

Llinás, R.R., and Steriade, M. (2006). Bursting of thalamic neurons and states of vigilance. Journal of Neurophysiology *95*, 3297-3308. 10.1152/jn.00166.2006.

Maingret, N., Girardeau, G., Todorova, R., Goutierre, M., and Zugaro, M. (2016). Hippocampo-cortical coupling mediates memory consolidation during sleep. Nature Neuroscience *19*, 959-964. 10.1038/nn.4304.

Mak-McCully, R.A., Rolland, M., Sargsyan, A., Gonzalez, C., Magnin, M., Chauvel, P., Rey, M., Bastuji, H., and Halgren, E. (2017). Coordination of cortical and thalamic activity during non-REM sleep in humans. Nature Communications *8*, 15499. 10.1038/ncomms15499.

McCormick, D.A., McGinley, M.J., and Salkoff, D.B. (2015). Brain state dependent activity in the cortex and thalamus. Current Opinion in Neurobiology *31*, 133-140.

Oostenveld, R., Fries, P., Maris, E., and Schoffelen, J.M. (2011). FieldTrip: Open source software for advanced analysis of MEG, EEG, and invasive electrophysiological data. Computational Intelligence and Neuroscience *2011*, 156869. 10.1155/2011/156869.

Pedroarena, C., and Llinás, R. (1997). Dendritic calcium conductances generate high-frequency oscillation in thalamocortical neurons. Proceedings of the National Academy of Sciences *94*, 724-728.

Piantoni, G., Halgren, E., and Cash, S.S. (2017). Spatiotemporal characteristics of sleep spindles depend on cortical location. NeuroImage *146*, 236-245.

Rosen, B.Q., and Halgren, E. (2022). An estimation of the absolute number of axons indicates that human cortical areas are sparsely connected. PLOS Biology *20*, e3001575. 10.1371/journal.pbio.3001575.

Rubin, D.B., Hosman, T., Kelemen, J.N., Kapitonava, A., Willett, F.R., Coughlin, B.F., Halgren, E., Kimchi, E.Y., Williams, Z.M., Simeral, J.D., et al. (2022). Learned motor patterns are replayed in human motor cortex during sleep. Journal of Neuroscience, JN-RM-2074-2021. 10.1523/jneurosci.2074-21.2022.

Salinas, E., and Sejnowski, T.J. (2001). Correlated neuronal activity and the flow of neural information. Nature Reviews Neuroscience *2*, 539-550.

Silber, M.H., Ancoli-Israel, S., Bonnet, M.H., Chokroverty, S., Grigg-Damberger, M.M., Hirshkowitz, M., Kapen, S., Keenan, S.A., Kryger, M.H., and Penzel, T. (2007). The visual scoring of sleep in adults. Journal of Clinical Sleep Medicine *3*, 121-131.

Stark, E., Roux, L., Eichler, R., Senzai, Y., Royer, S., and Buzsáki, G. (2014). Pyramidal cell-interneuron interactions underlie hippocampal ripple oscillations. Neuron *83*, 467-480. 10.1016/j.neuron.2014.06.023.

Varela, C., Kumar, S., Yang, J.Y., and Wilson, M.A. (2014). Anatomical substrates for direct interactions between hippocampus, medial prefrontal cortex, and the thalamic nucleus reuniens. Brain Structure and Function *219*, 911-929. 10.1007/s00429-013-0543-5.

Vaz, A.P., Inati, S.K., Brunel, N., and Zaghloul, K.A. (2019). Coupled ripple oscillations between the medial temporal lobe and neocortex retrieve human memory. Science *363*, 975-978. 10.1126/science.aau8956.

Vaz, A.P., Wittig, J.H., Inati, S.K., and Zaghloul, K.A. (2020). Replay of cortical spiking sequences during human memory retrieval. Science *367*, 1131-1134. 10.1126/science.aba0672.

Vicente, R., Gollo, L.L., Mirasso, C.R., Fischer, I., and Pipa, G. (2008). Dynamical relaying can yield zero time lag neuronal synchrony despite long conduction delays. Proceedings of the National Academy of Sciences *105*, 17157-17162.

Wilson, M.A., and McNaughton, B.L. (1994). Reactivation of hippocampal ensemble memories during sleep. Science *265*, 676-679. 10.1126/science.8036517.

Xuereb, J.H., Perry, R.H., Candy, J.M., Perry, E.K., Marshall, E., and Bonham, J.R. (1991). Nerve cell loss in the thalamus in Alzheimer's disease and Parkinson's disease. Brain *114 (Pt 3)*, 1363-1379.